Radiation Measurements 106 (2017) 73–78

Contents lists available at ScienceDirect

Radiation Measurements

journal homepage: www.elsevier.com/locate/radmeas

Radio-photoluminescence in Sm-doped BaF_2-Al_2O_3-B_2O_3 glass-ceramics

Go Okada [a,*], Kenji Shinozaki [b,c], Takayuki Komatsu [c], Safa Kasap [d], Takayuki Yanagida [a]

[a] Graduate School of Materials Science, Nara Institute of Science and Technology (NAIST), 8916-5 Takayama, Ikoma, Nara 630-0192, Japan
[b] National Institute of Advanced Industrial Science and Technology (AIST), 1-8-31 Midorigaoka, Ikeda, Osaka 563-8577, Japan
[c] Department of Materials Science and Technology, Nagaoka Institute of Technology, 1603-1 Kamitomioka-cho, Nagaoka, Niigata 940-2188, Japan
[d] Department of Electrical and Computer Engineering, University of Saskatchewan, 57 Campus Dr., Saskatoon, SK S7N5A9, Canada

HIGHLIGHTS

- Glass ceramics consisting of $BaAlBO_3F_2$:Sm crystallites were obtained.
- RPL was observed in $BaAlBO_3F_2$:Sm due to $Sm^{3+} \rightarrow Sm^{2+}$ valence change.
- The RPL sensitivity was confirmed as low as 10 mGy.

ARTICLE INFO

Article history:
Received 29 July 2016
Received in revised form
24 November 2016
Accepted 14 December 2016
Available online 15 December 2016

Keywords:
Radio-photoluminescence
RPL
BaF_2-Al_2O_3-B_2O_3
Glass ceramics
Sm
X-rays

ABSTRACT

In this research we have found that Sm-doped BaF_2-Al_2O_3-B_2O_3 glass ceramics show radio-photoluminescence (RPL) properties associated with X-ray irradiation. Before X-ray irradiation, the photoluminescence (PL) emission is only due to the 4f-4f transitions of Sm^{3+} observed around 600 nm; however, after X-ray irradiation it shows additional PL emissions due to the 4f-4f transitions of Sm^{2+}. We attributed the origin of this RPL due to the inter-valence conversion of Sm ion ($Sm^{3+} \rightarrow Sm^{2+}$). The glass ceramic sample includes $BaAlBO_3F_2$ crystallites in the glass matrix, and the RPL is only valid for Sm included in the crystalline phase since the precursor glass (without the crystalline phase) does not show RPL. The RPL response is so stable that it does not show any indication of fading even by heating at high temperatures up to 400 °C. For radiation sensing applications, we have confirmed that it shows a monotonically increasing response with X-ray dose at least over the 10–10,000 mGy; and it has been demonstrated for 2D dosimetry applications.

1. Introduction

Phosphor materials are often used for radiation measurements (Knoll, 2010). A scintillator is a common example, which is well known to emit light instantly as a result of interacting with incident radiation. In contrast, storage phosphors are also used for radiation sensing for its distinct advantages; for example, it does not require external circuits and batteries during radiation sensing. Thermally-stimulated luminescence (TSL) (McKeever, 1985) and optically-stimulated luminescence (OSL) (Yukihara and McKeever, 2011) are well characterized radiation-induced phenomena in storage phosphors and widely used for dosimetry applications such as personnel dose monitoring (McKinlay, 1981) and X-ray imaging (Rowlands, 2002). In recent years, in contrast, there are growing scientific and practical interests in so-called radio-photoluminescence (RPL). RPL is a phenomenon seen in phosphors that irradiation generates luminescent centres; therefore, photoluminescence (PL) intensity represents the concentration of centers created and hence the amount radiation dose delivered (Belev et al., 2011). The radiation-generated luminescent centres are typically so stable that, unlike TSL and OSL, one can read out the signal multiple times without experiencing fading of signal and it allows us to utilize fluorescent microscopy readout in order to achieve sub-micrometer image resolution (Akselrod and Akselrod, 2006; Kurobori et al., 2016; Okada et al., 2011). Despite these distinct advantages, there are not many materials known to show RPL today. Some selected materials are: LiF (Levita et al., 1976), Ag-doped phosphate glasses (Yokota and Imagawa, 1967), Al_2O_3:C,

* Corresponding author.
E-mail address: go-okada@ms.naist.jp (G. Okada).

http://dx.doi.org/10.1016/j.radmeas.2016.12.006
1350-4487/

Mg (Akselrod et al., 2003), and Sm-doped crystals, glasses, and glass-ceramics (Belev et al., 2011; Martin et al., 2013; Morrell et al., 2014; Okada et al., 2014, 2013, 2011; Vahedi et al., 2012).

In the present work, we have synthesized and characterized BaF_2-Al_2O_3-B_2O_3 glass ceramics for novel radiation dosimetry applications. Previously, Shinozaki et al. (Shionozaki et al., 2012) has reported that $BaAlBO_3F_2$ crystals formed in $50BaF_2$-$25Al_2O_3$-$25B_2O_3$ glass by heat-treatment and single crystal line can be induced on the surface of the glass doped with NiO by using a laser induced crystallization technique, which allows us to draw optical light guides in glass. Note that the glass composition corresponds to the stoichiometric composition of $BaAlBO_3F_2$. Shinozaki et al. (2014) has also reported that Eu^{3+}-doped BaF_2-Al_2O_3-B_2O_3 glasses exhibit highly efficient red PL up to ~97% of quantum yield and small concentration quenching. Tao et al. (2014) has reported that Eu^{2+}-doped $BaAlBO_3F_2$ crystal shows high efficient blue PL with 72% of quantum yield. These reports indicate that rare earth doped BaF_2-Al_2O_3-B_2O_3 glasses and glass-ceramics with $BaAlBO_3F_2$ crystals have high potential as efficient phosphors. The aim of this paper is synthesis, characterizations, and radiation dosimetry applications of Sm-doped BaF_2-Al2O3-B_2O_3 glass system.

2. Materials and methods

$1Sm_2O_3$-doped $50BaF_2$-$25Al_2O_3$-$25B_2O_3$ (in mol%) glass-ceramics were synthesized as follows. Reagent grade powders of Sm_2O_3, BaF_2, Al_2O_3 and B_2O_3 were mixed first, and the mixture (10 g batch) was then loaded in a Pt crucible and melted at 1200 °C for 20 min in an electric furnace. Next, the melt was poured on to an iron plate and pressed by another plate to fabricate a glass plate with the thickness of ~1 mm. After mechanically polished to mirror finish with CeO_2 powder, the as-prepared glass samples were heat-treated at a series of temperatures (500, 510, 525, and 550 °C) for 3 h by means of nucleation and growth of $BaAlBO_3F_2$ crystalline phase, and to obtain glass-ceramics.

Glass transition (T_g) and crystallization (T_x) temperatures of as-synthesized glass were characterized by differential thermal analysis (DTA; Thermo plus TG8120, Rigaku), with a heating rate of 10 °C/min. The presence of crystallites and crystalline structures in heat-treated glass samples were confirmed using a powder X-ray diffractometer (XRD; MiniFlex 600, Rigaku). Also, we have observed the surface of the samples with scanning electron microscopy (SEM; JSM-6510, JEOL) for verification of the crystalline phase and to estimate the approximate grain size. For the SEM measurement, sample surface was chemically etched by soaking in 1N-HCl for 3 min.

Optical transmittance was measured by using a spectrophotometer (V-670, JASCO). PL emission and excitation spectra were measured using a spectrofluorormeter (FP8600, JASCO). RPL as an X-ray induced response was measured using a separate experimental setup. Here, as an excitation source, a Xenon lamp (LAX-C100, Asahi Spectra) was used with a combination of bandpass filter to obtain a 340 nm excitation light, which was delivered to the sample. Upon PL excitation, the emission light was collected by a fibre-coupled lens and guided to a CCD-based spectrometer (QEPro, Ocean Optics) to digitize the PL spectrum. The RPL response was defined as: $Response = I_1(650–750\ \mathrm{nm}) - I_0(650–750\ \mathrm{nm})$ where the former and latter terms are integrated PL intensities over 650–750 nm of irradiated and non-irradiated samples, respectively. X-ray irradiations were carried out using an X-ray generator (XRBOP&N200X4550, Spellman), which was equipped with a conventional X-ray tube with a W anode and Be window. The applied voltage was fixed to 40 kVp. The representation of X-ray dose used throughout this paper is dose in air at the entrance of sample.

3. Results and discussion

Fig. 1 shows Sm-doped BaF_2-Al_2O_3-B_2O_3 samples with different heat-treatment histories. It is clearly seen that the sample colour becomes milky with increasing heat-treatment temperature. The one annealed at 525 °C is still seen translucent while the one annealed at 550 °C is almost completely opaque.

Fig. 2 shows in-line transmittance spectra of Sm-doped BaF_2-Al_2O_3-B_2O_3 samples with different heat-treatment histories. On one hand, it is clearly seen that the as-prepared glass sample and annealed samples at 500 and 510 °C are very transparent in the near-UV, visible, and near infrared regions with some absorption features by Sm^{3+} ions; and these spectra have no significant difference. On the other hand, the ones annealed at higher temperatures (525 and 550 °C) show much less transmittance. The transmitted intensity decreases as the absorption edge shifts towards longer wavelengths with increasing heat-treatment temperature. The latter behaviour is typical for Mie-scattering, in which size of the scattering centres is equivalent or larger than the wavelength and light scattering is independent of the wavelength. This result is consistent with visual observation of the samples shown in Fig. 1 where the samples annealed at 525 and 550 °C look milky due to significant scattering of light. It should be also pointed out that there are notable difference in refractive indices between the glass matrix and crystal (Shionozaki et al., 2012), otherwise the $BaAlBO_3F_2$ crystallites do not act as scattering centres.

Fig. 3 shows DTA thermogram recorded for Sm-doped BaF_2-Al_2O_3-B_2O_3 glass. The glass transition temperature (T_g) was clearly

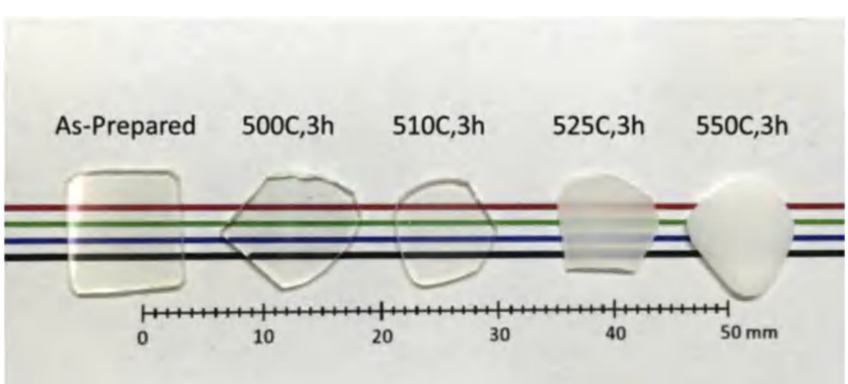

Fig. 1. Synthesized samples with different heat-treatment histories.

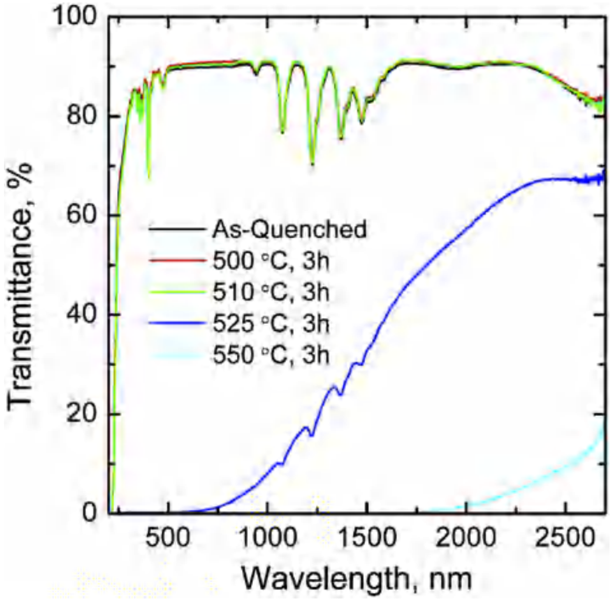

Fig. 2. Transmittance spectra of Sm-doped BaF_2-Al_2O_3-B_2O_3 samples with different heat-treatment histories.

detected around 490 °C, and there is an intense exothermal peak around 575 °C. The latter peak temperature is about 10 °C higher than the value reported earlier (Shionozaki et al., 2012); and the previous work pointed out that this exothermal peak corresponds to an bulk crystallization of $BaAlBO_3F_2$ crystalline phase, and the crystallization mechanism is bulk crystallization. Shinozaki et al. proposed that the glass is composed of similar structure units, i.e., BO_3 and $Al(O,F)_x$ units without non-bridging oxygen (Shinozaki et al., 2014). The structural similarity indicates the phase transition rate would be high. Since the previously reported data were measured with a sample without any rare earth dopant, it is possible that the addition of Sm_2O_3 has somewhat increased the crystallization temperature.

Fig. 4 shows XRD patterns of Sm-doped BaF_2-Al_2O_3-B_2O_3 samples with different heat-treatment histories. Also, at the bottom of the figure, XRD card pattern of $BaAlBO_3F_2$ (PDF #8100293) is represented. The XRD data clearly indicates that the sample remains glass for those without heat-treatment and annealed at lower temperatures whereas $BaAlBO_3F_2$ crystalline phase appears for those annealed at 525 °C and higher temperatures. Furthermore, comparing between those annealed at 525 °C and 550 °C, the diffraction intensities are much more pronounced for the latter sample.

Fig. 5 shows SEM images of Sm-doped BaF_2-Al_2O_3-B_2O_3 samples annealed at (a) 510 °C, (b) 525 °C, and (c) 550 °C for 3 h. The image of the sample annealed at 510 °C looks relatively smooth but there are some noticeable bright spots with negligibly small diameter (estimated ~0.2 μm^2 on average). It is not easy to identify by EDS what these spots are because the glass and $BaAlBO_3F_2$ are related (stoichiometric) composition, but some possibilities are: (a) the particles are so small and little compared to the entire volume that the signal was below the detection limit in XRD; and (b) separated phase of host matrix. With increasing heat-treatment temperature, the structure becomes much more pronounced. Since the XRD measurements showed clear diffraction patterns of $BaAlBO_3F_2$ for annealed samples at 525 and 550 °C, these considerable features seen in Fig. 5 (b) and (c) are attributed to $BaAlBO_3F_2$ crystallites. When annealed at 525 °C, the average crystalline size is approximately ~0.6 μm^2. When annealed at 550 °C, the SEM image is almost entirely covered by crystalline grains with the average size of ~2 μm^2.

Fig. 6 shows PL emission spectra of Sm-doped BaF_2-Al_2O_3-B_2O_3 glass-ceramic samples irradiated by different X-ray doses, 0, 1, and 10 Gy. The excitation wavelength used here is 340 nm. The spectra are normalized to the peak intensity around 650 nm to become unity. Without any X-ray irradiation, the sample shows PL emissions only due to the 4f-4f transitions of Sm^{3+}. After X-ray irradiation, additional emissions are observed mainly around 700 nm; and the intensity increases with increasing irradiation dose. For the spectral positions, it is reasonable to attribute these emissions due to the 4f-4f transitions of Sm^{2+}. The attributions are also supported

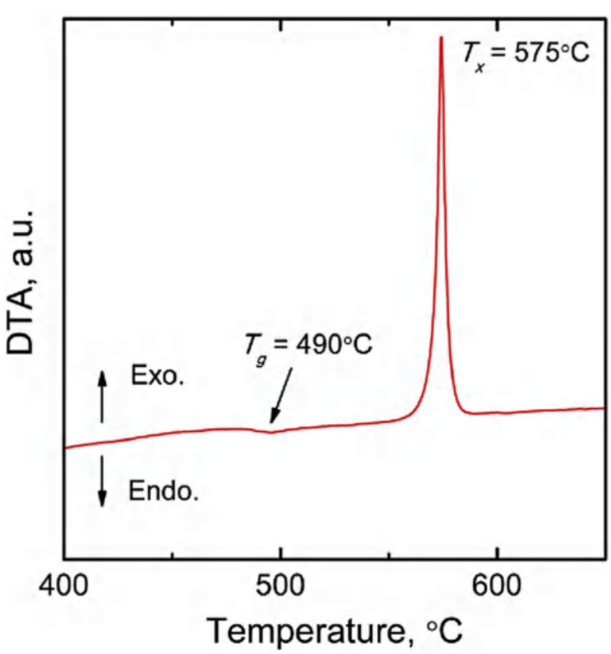

Fig. 3. DTA thermogram of as-prepared Sm-doped BaF_2-Al_2O_3-B_2O_3 glass.

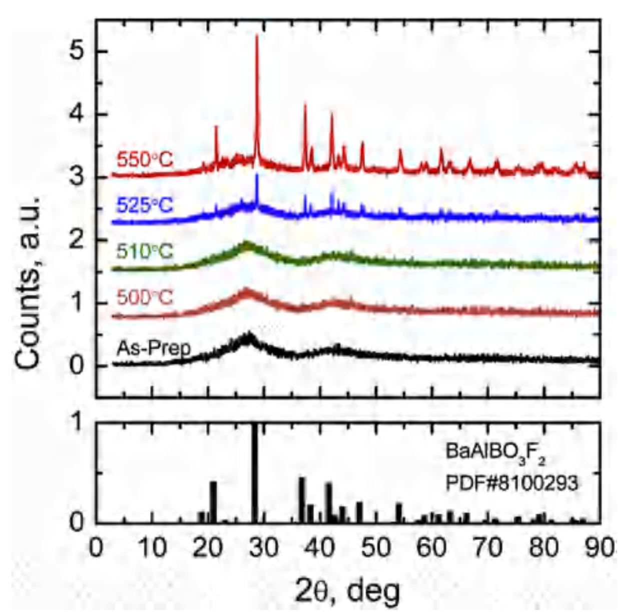

Fig. 4. XRD patterns of Sm-doped BaF_2-Al_2O_3-B_2O_3 samples with different heat-treatment histories.

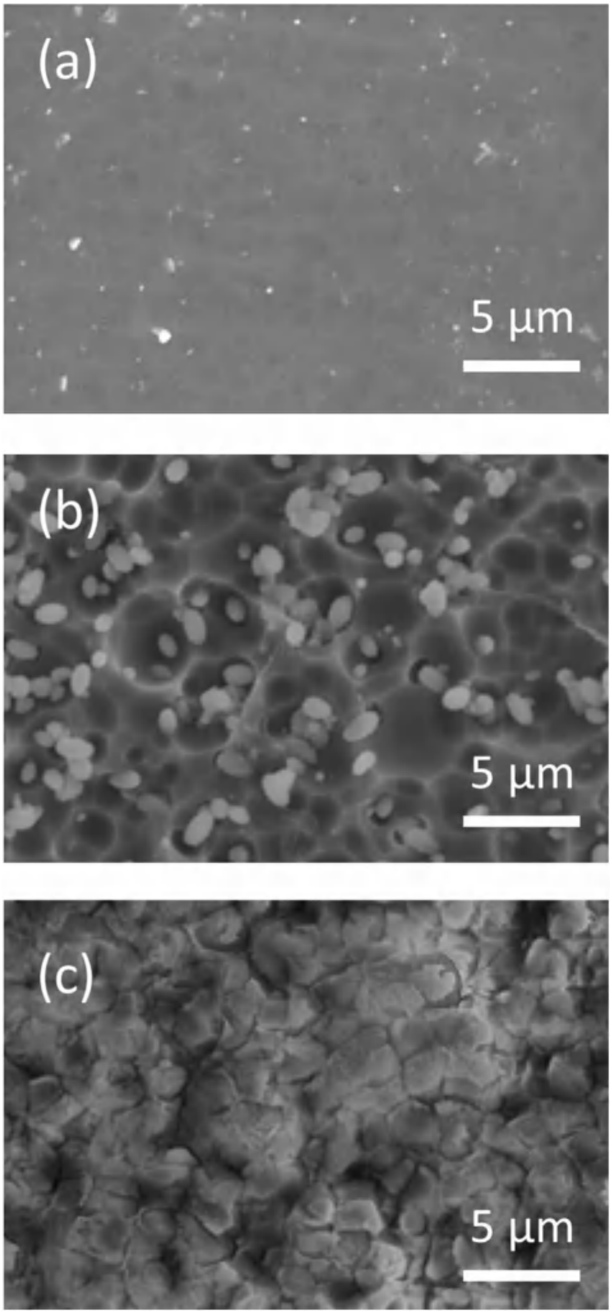

Fig. 5. SEM images of Sm-doped BaF_2-Al_2O_3-B_2O_3 samples with different heat-treatment histories: (a) 510 °C, (b) 525 °C, and (c) 550 °C for 3 h.

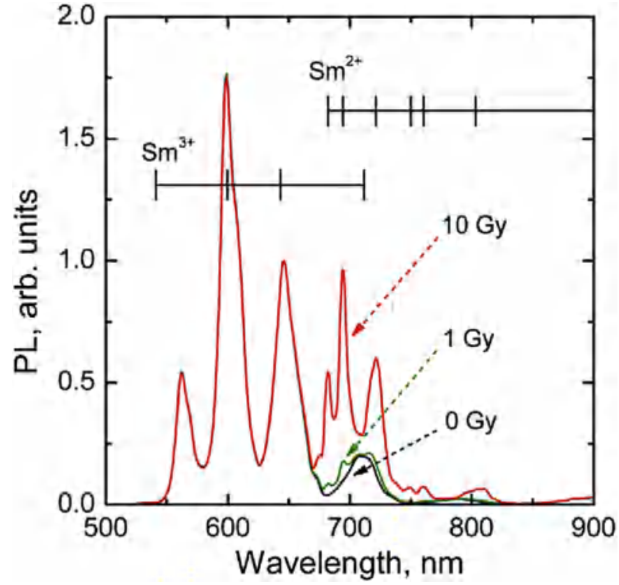

Fig. 6. PL emission spectra of Sm-doped BaF_2-Al_2O_3-B_2O_3 glass-ceramic samples as a function of X-ray irradiation dose. The heat-treatment conditions are: 550 °C for 3 h. The PL excitation wavelength is 340 nm.

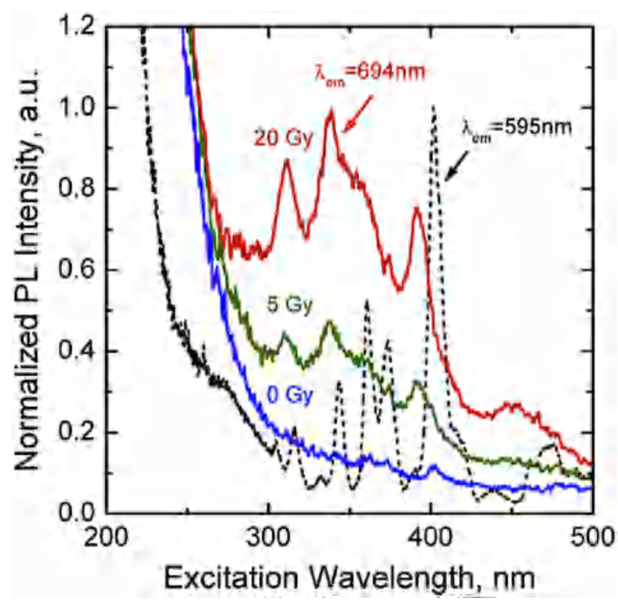

Fig. 7. PL excitation spectra of Sm-doped BaF_2-Al_2O_3-B_2O_3 glass-ceramic sample (550 °C, 3 h) as a function of irradiation dose.

by excitation spectrum. Fig. 7 shows PL emission and excitation spectra of Sm-doped BaF_2-Al_2O_3-B_2O_3 glass-ceramic sample (550 °C, annealed for 3 h). The excitation spectrum of the Sm^{3+} emission shows typical sharp line features while the excitation spectrum of the emission at 694 nm has very broad feature. Such broad excitation feature is commonly seen in Sm^{2+}-doped phosphors due to its parity-allowed 4f-5d transitions. For these reasons, in this material system we have intervalence conversion of Sm ion ($Sm^{3+} \rightarrow Sm^{2+}$) induced by X-ray irradiation; and it can be observed as the appearance of PL emissions by Sm^{2+} which increases as a function of irradiation dose. In other words, new luminescent centres (Sm^{2+}) are generated by X-ray irradiation, so the phenomenon involved here is RPL. It should be noted here that the RPL can only be observed in the samples annealed at 525 and 550 °C, which include $BaAlBO_3F_2$ crystallites. Therefore, we think that some of Sm ions are embedded in the crystals and RPL is only effective in the crystalline environment. As illustrated in Fig. 8, the RPL response was confirmed to increase monotonically against the incident X-ray dose over 10–10,000 mGy. The lower end is due to detection limit of the measurement instrument while the X-ray generator used here can only deliver continuous irradiation up to 10 Gy.

Fig. 9 demonstrates the capability of Sm-doped BaF_2-Al_2O_3-B_2O_3 glass-ceramic sample (550 °C, 3 h) to be used for X-ray imaging applications. The glass-ceramic samples were irradiated through Pb resolution targets with different spatial frequencies: (a) 0.5, (b) 1.5,

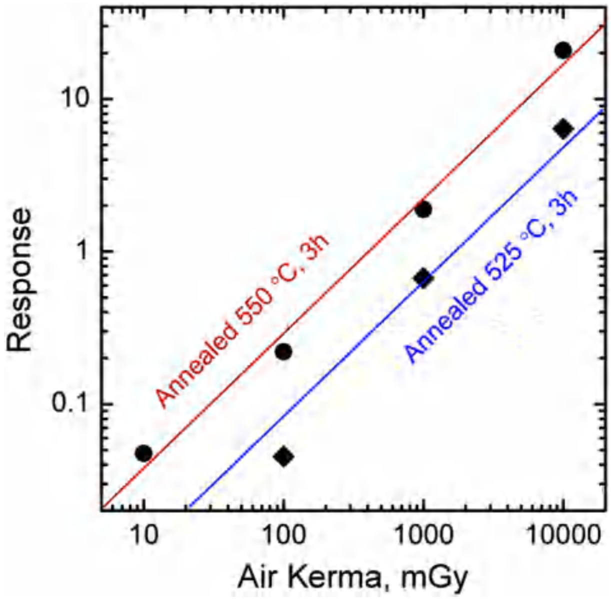

Fig. 8. RPL response of Sm-doped BaF_2-Al_2O_3-B_2O_3 glass-ceramic sample (550 °C, 3 h) as a function of X-ray irradiation dose.

(c) 2.5, (d) 4.0, and (e) 5.0 lp/mm. The contrasts (or modulation transfer function; MTF) of X-ray images are evaluated as MTF = $(I_{max} - I_{min})/(I_{max} + I_{min})$ where I_{max} is the measured intensity of irradiated lines, that is in bright bands, and I_{min} is the intensity in the dark bands. The obtained values from each image are plotted in Fig. 9 (f). Overall, the MTF values are found to be not impressively high. We think the reason arises mainly from the irradiation geometry because the X-ray generator is not equipped with a collimator and the distance between the W target and sample was only ~10 cm. Despite the unfavorable irradiation geometry conditions, the 5.0 lp/mm lines (100 μm per line) are still reasonably resolved.

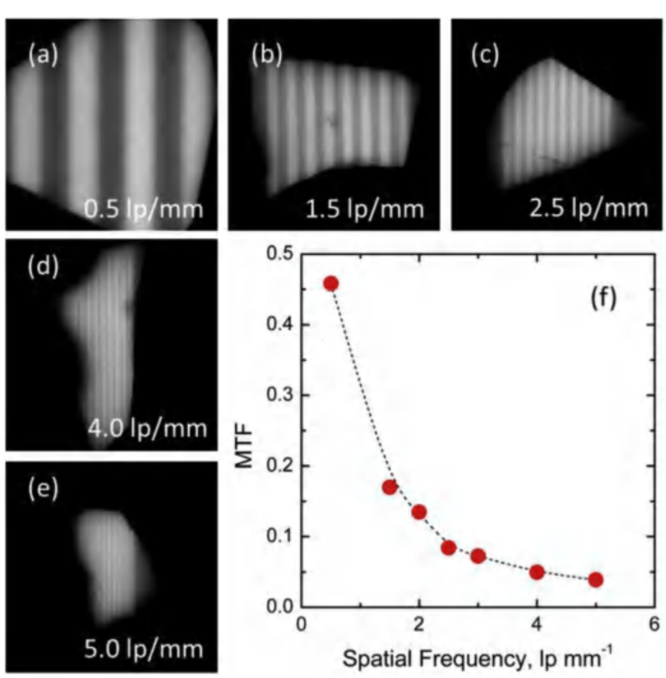

Fig. 9. Demonstration of spatial resolution in X-ray imaging applications.

4. Conclusion

We have synthesized Sm-doped BaF_2-Al_2O_3-B_2O_3 glass-ceramics and characterized basic material properties and RPL properties for radiation measurement applications. The glass-ceramics are fabricated by heat-treating melt-quenched glass solution. The as-quenched glass shows an intense exothermal peak around 575 °C in DTA thermogram, which corresponds to nucleation and growth of Sm:$BaAlBO_3F_2$ crystallites. Observations by XRD and SEM confirmed that the crystalline phase is present in the glass matrix when the as-quenched sample is annealed at 525 and 550 °C for 3 h. The average crystalline sizes are ~0.6 and 2 μm^2, respectively. PL measurement of glass-ceramic sample before and after X-ray irradiation revealed that originally doped Sm^{3+} is reduced to Sm^{2+}. As a result, Sm^{2+} act as luminescent centre (in addition to Sm^{3+}) and the PL intensity from Sm^{2+} monotonically increases as a function of delivered X-ray dose. Using the latter RPL phenomenon, 2D dosimetry was successfully demonstrated and confirmed that 5 lp/mm (100 μm) is reasonably resolvable with a basic reader setup.

Acknowledgement

This research was co-supported by a Grant-in-Aid for Scientific Research (A) (26249147) and Grant-in-Aid for Research Activity start-up (15H06409) from the Ministry of Education, Culture, Sports, Science and Technology of the Japanese government (MEXT). It is also partially supported by the Adaptable and Seamless Technology transfer Program (A-STEP) by the Japan Science and Technology Agency, the Murata Science Foundation, Hitachi Metals Materials Science Foundations, and a cooperative research project of the Research Institute of Electronics, Shizuoka University.

References

Akselrod, M.S., Akselrod, A.E., 2006. New Al_2O_3:C,Mg crystals for radiophotoluminescent dosimetry and optical imaging. Radiat. Prot. Dosim. 119, 218–221. http://dx.doi.org/10.1093/rpd/nci663.

Akselrod, M.S., Akselrod, a.E., Orlov, S.S., Sanyal, S., Underwood, T.H., 2003. Fluorescent aluminum oxide crystals for volumetric optical data storage and imaging applications. J. Fluoresc. 13, 503–511. http://dx.doi.org/10.1023/B:JOFL.0000008061.71099.55.

Belev, G., Okada, G., Tonchev, D., Koughia, C., Varoy, C., Edgar, A., Wysokinski, T., Chapman, D., Kasap, S., 2011. Valency conversion of samarium ions under high dose synchrotron generated X-ray radiation. Phys. Status Solidi 8, 2822–2825. http://dx.doi.org/10.1002/pssc.201084103.

Knoll, G.F., 2010. Radiation Detection and Measurement, fourth ed. Wiley.

Kurobori, T., Yanagida, Y., Chen, Y.Q., 2016. A three-dimensional imaging detector based on nano-scale silver-related defects in X- and gamma-ray-irradiated glasses. Jpn. J. Appl. Phys. 55, 02BC01. http://dx.doi.org/10.7567/JJAP.55.02BC01.

Levita, M., Schlesinger, T., Friedland, S.S., 1976. LiF dosimetry based on radiophotoluminescence (RPL). IEEE Trans. Nucl. Sci. 23, 667–674. http://dx.doi.org/10.1109/TNS.1976.4328325.

Martin, V., Okada, G., Tonchev, D., Belev, G., Wysokinski, T., Chapman, D., Kasap, S., 2013. Samarium-doped oxyfluoride borophosphate glasses for x-ray dosimetry in Microbeam Radiation Therapy. J. Non. Cryst. Solids 377, 137–141. http://dx.doi.org/10.1016/j.jnoncrysol.2012.12.015.

McKeever, S.W.S., 1985. Thermoluminescence of Solids. Cambridge University Press.

McKinlay, A.F., 1981. Thermoluminescence Dosimetry (Medical Physics Handbook 5). Heyden & Sons Inc., Philadelphia.

Morrell, B., Okada, G., Vahedi, S., Koughia, C., Edgar, a., Varoy, C., Belev, G., Wysokinski, T., Chapman, D., Sammynaiken, R., Kasap, S.O., 2014. Optically erasable samarium-doped fluorophosphate glasses for high-dose measurements in microbeam radiation therapy. J. Appl. Phys. 115, 63107. http://dx.doi.org/10.1063/1.4864424.

Okada, G., Morrell, B., Koughia, C., Edgar, A., Varoy, C., Belev, G., Wysokinski, T., Chapman, D., Kasap, S., 2011. Spatially resolved measurement of high doses in microbeam radiation therapy using samarium doped fluorophosphate glasses. Appl. Phys. Lett. 99, 121105. http://dx.doi.org/10.1063/1.3633102.

Okada, G., Ueda, J., Tanabe, S., Belev, G., Wysokinski, T., Chapman, D., Tonchev, D., Kasap, S., 2014. Samarium-doped oxyfluoride glass-ceramic as a new fast erasable dosimetric detector material for microbeam radiation cancer therapy applications at the canadian synchrotron. J. Am. Ceram. Soc. 97, 2147–2153. http://dx.doi.org/10.1111/jace.12938.

Okada, G., Vahedi, S., Morrell, B., Koughia, C., Belev, G., Wysokinski, T., Chapman, D., Varoy, C., Edgar, A., Kasap, S., 2013. Examination of the dynamic range of Sm-doped glasses for high-dose and high-resolution dosimetric applications in microbeam radiation therapy at the Canadian synchrotron. Opt. Mat.Amst.t) 35, 1976–1980. http://dx.doi.org/10.1016/j.optmat.2012.10.049.

Rowlands, J.A., 2002. The physics of computed radiography. Phys. Med. Biol. 47, R123–R166. http://dx.doi.org/10.1088/0031-9155/47/23/201.

Shinozaki, K., Honma, T., Komatsu, T., 2014. High quantum yield and low concentration quenching of Eu^{3+} emission in oxyfluoride glass with high BaF_2 and Al_2O_3 contents. Opt. Mat.Amst.t) 36, 1384–1389. http://dx.doi.org/10.1016/j.optmat.2014.03.037.

Shionozaki, K., Honma, T., Komatsu, T., 2012. New oxyfluoride glass with high fluorine content and laser patterning of nonlinear optical $BaAlBO_3F_2$ single crystal line. J. Appl. Phys. 112, 3–10. http://dx.doi.org/10.1063/1.4764326.

Tao, Z., Huang, Y., Cai, P., Kim, S., Il Seo, H.J., 2014. Synthesis and efficient blue-emitting of Eu^{2+}-activated borate fluoride $BaAlBO_3F_2$. Opt. Mat.Amst.t) 37, 287–292. http://dx.doi.org/10.1016/j.optmat.2014.06.010.

Vahedi, S., Okada, G., Morrell, B., Muzar, E., Koughia, C., Edgar, A., Varoy, C., Belev, G., Wysokinski, T., Chapman, D., Kasap, S., 2012. X-ray induced Sm^{3+} to Sm^{2+} conversion in fluorophosphate and fluoroaluminate glasses for the monitoring of high-doses in microbeam radiation therapy. J. Appl. Phys. 112 http://dx.doi.org/10.1063/1.4754564.

Yokota, R., Imagawa, H., 1967. Radiophotoluminescent centers in silver-activated phosphate glass. J. Phys. Soc. Jpn. 23, 1038–1048. http://dx.doi.org/10.1143/JPSJ.23.1038.

Yukihara, E.G., McKeever, S.W.S., 2011. Optically Stimulated Luminescence. John Wiley & Sons, Ltd, Chichester, UK. http://dx.doi.org/10.1002/9780470977064.